Analysis of Stress and Strain in Sandwich Structures Using an Equivalent Finite Element Model

Lien Tien Dao, Pham Tuong Minh Duong, Viet Dung Luong*

Faculty of Mechanical Engineering, Thai Nguyen University of Technology, Thai Nguyen Province, Viet Nam

Received 24 April 2024; received in revised form 17 June 2024; accepted 19 June 2024

DOI: https://doi.org/10.46604/ijeti.2024.13630

Abstract

The study aims to build an equivalent 2D model as an alternative to the 3D model of sandwich panel structures. This model enables for reducing model building time and calculation time in the design calculation of this sandwich structure. The research object in this study is corrugated core cardboard. First, the isotropic plasticity equivalent (IPE) model for the paper material is implemented in the Abaqus software, using the VUMAT user subroutine. Subsequently, the homogenization method is proposed as an equivalent elastic-plastic finite element model. This model is implemented in Abaqus using the UGENS subroutine. Finally, numerical simulations of different load cases between the 3D model and the equivalent 2D model are performed to confirm the accuracy of the proposed model. The comparison results indicate that the equivalent model ensures exceptional accuracy compared to the 3D model but significantly reduces model building time and CPU time.

Keywords: finite element, homogenization, equivalent model, sandwich

1. Introduction

In the process of designing and developing products, a constant need emerges to expedite design procedures, cut costs, and ensure technical criteria such as durability, hardness, etc., especially for complex structures. Studying mechanical behavior and establishing appropriate calculation models are the requisites. Complex structures subjected to varying loads such as sandwich panels are extensively applied in both industrial and civil construction. Over time, published studies related to the mechanical behavior of sandwich panels have been profusely presented. Specifically, these studies employ sundry research methodologies, including experimental research, the combination of experimental research and numerical simulation, and homogeneous modeling. Sandwich panel structures are composite structures with complex behavior. This behavior results from many D-regions, which are considered the foundation behind non-linear behavior and failed initiation. Such a behavior hampers analytical methods to simulate this behavior. One of the most powerful techniques is to use the finite element method [1-2].

Simultaneously, a 3D finite element model was also established for numerical simulation [3]. The specific energy absorption of the panels exhibited a similitude between experimental results and numerical simulations. Computational and experimental methods were employed to study the response of sandwich steel beams with corrugated cores to quasi-static loads [4], in corrugated core sandwich panels [5]. Some studies pertinent to paper and cardboard focus on analyzing and determining bending stiffness based on known parameters of the constituting paper types and the geometry of the corrugated layers [6], developing an algorithm to recognize accurate geometric shape features of corrugated double-core cardboard

* Corresponding author. E-mail address: luongvietdung@tnut.edu.vn

English language proofreader: Chih-Wei Chang

through integrating image processing and genetic algorithms [7], the influence of the complexity of transverse folds on the in-plane deformation accuracy is included in the finite element model [8]. In addition, a failure model for creasing and folding paperboard was also developed [9]. The edge compression tests and box compression tests were performed directly on corrugated cardboard structures to evaluate the compression resistance under stacking conditions of carton boxes.

Simultaneously, the finite element modeling (FEM) model was also developed to serve as a basis for comparing and evaluating experimental results [10]. The results are compared with numerical predictions given by finite element analysis (FEA) and results germane to analytical modeling. FEA predictions generally manifest fairly apposite agreement with experimental measurements. Studies using a combination of experiments and numerical simulations have attested that experiments on sandwich panel structures can be completely replaced by experimental numerical simulations. However, in apropos the models with large sizes and complex structures, the numerical simulation time is considerable.

To solve this problem, one approach to studying the mechanical behavior of sandwich structures is using homogenization techniques to develop an equivalent model as a substitute for the 3D model. Legion homogenization methods have been developed, whereas each method only solves certain problems such as compressive, bending, and torsional loads. The equivalent 2D model is built based on the Mindlin–Reissner plate theory to analyze the linear behavior [11], on Hill's criteria for natural orthotropic materials and Ilyushin criterion for isotropic plates, and shells are combined to analyze the elastoplastic of corrugated core sandwich panels [12], by using the asymptotic expansion method [13]. The accuracy of the 2D model is verified through a comparison of the response of the real plate and its closely equivalent model under pure bending loads. Furthermore, for similar structures, an approach based on the use of unit cells using the finite element method has been developed to avoid geometric modeling of the entire structure and reduce the time calculation [14-15].

The elastic-plastic behavior of cardboard plates in the layers of corrugated core cardboard is mentioned by Stenberg [16]. This model enables the simulation of elastic-plastic behavior under high compressive loading in the through-thickness direction (ZD). An elastic-plastic material model for the in-plane mechanical properties of paper material was introduced by Mäkelä and Östlund [17]. Aboura et al. [18] established a homogenization model to investigate the elastic behavior of a single corrugated cardboard sheet using the integration method. The integration method when establishing an elastic homogeneity model for double corrugated corrugated cardboard sheets was also established in Duong's research [19]. Given the investigations listed above, homogenization models that use the integration method yield high accuracy and have been applied to calculate practical problems such as numerical simulation to calculate fatigue strength for carton boxes subjected to cyclic load [20], and numerical simulation for free drop test of corrugated carton packaging [21].

Depending on each research approach, equivalent models are built using different methods. A numerical homogenization method based on the equivalence of elastic energy between a representative volume element and an equivalent plate was developed. This approach considers these imperfections when creating a simplified model. Finally, an initial defect pattern was proposed, which most accurately reflects the decrease in sheet stiffness [22]. The homogeneous model in which the material behavior is anisotropic has been included in the equivalent model for the core of corrugated iron sheets [23]. The equivalent properties of the materials in the model are calculated through mathematical expressions including the influence of fold shape, layer angle, layer thickness, and fiber volume ratio.

Zhang et al. [24] also developed an equivalent FEM method for sandwich panels. This model is applied to study the plastic-forming process of bi-directional trapezoidal sandwich (BTS) and aluminum foam sandwich (AFS) panels. Barrett [25] deployed a simple high-order theory for FEA of homogeneous and multi-layer composite panels. The homogenization model considers the effect of stiffness loss related to wrinkling and/or perforation of the corrugated core board [26], Meanwhile, the cross-sectional stiffness is built based on the equivalence of strain energy between the full 3D numerical model of the carton sheet and the Reissner-Mindlin flat sheet representation [27]. In addition to equivalent 2D models, some studies build

equivalent 3D models. A simple equivalent 3D finite element model is regarded as an alternative to a full 3D model to predict the elastic behavior of cardboard panels [28] and to consider the influence of geometric parameters on the elastic behavior of corrugated core cardboard [29].

The erstwhile studies indicate that a myriad of equivalent models have been developed to replace models when inspecting the behavior of corrugated core sandwich panels. However, most of the published research is limited to models investigating the elastic behavior of materials. These models do not mention computational simulation time. Especially in verifying the accuracy of the model, the load cases corresponding to the change in stress and strain have not been fully considered. In this study, an equivalent elastic-plastic model is proposed to study the mechanical behavior of corrugated cardboard structures, especially the change in stress-strain in this structure when subjected to changing loads. Moreover, calculation time is also included in the proposed model.

The article is divided into five sections. Section 1 discusses an overview of research issues and the remaining issues that need to be resolved. Section 2 presents important theoretical foundations for building the model. In Session 3, an equivalent elastic-plastic model is built to study the change of stress-strain for corrugated cardboard sheets when subjected to load. Section 4 evaluates and confirms the results obtained and expands the model to study other issues. Session 5 discusses the equivalent elastic-plastic model, which aims to completely solve problems related to calculation speed and cost reduction in the calculation and design process of sandwich panel structures.

2. Methodology

In this section, shell plate theories along with relevant symbols will be introduced. Especially the isotropic plasticity equivalent (IPE) model of paper material. This behavior model is not available in the Abaqus software library and therefore must be implemented in Abaqus using the VUMAT subroutine. Since the aforementioned conditions are important foundations for conducting the assimilation method and for conducting the method of homogenizing corrugated cardboard panels.

2.1. Description of symbol

An equivalent 2D model is established to replace the 3D model of carton sheets using the homogenization method. This method is based on published theories, through mathematical equations, matrices, and tensors. Thus, before diving into the extensive research, the key terms and symbols, as enumerated in Table 1, are material for this study.

Table 1 Description of symbol

Sign	Symbol description
A_{ij}	The stiffness of the membrane
A, B, C, D, E_0, n	The parameters of the IPE model
B_{ij}	The coupling between membrane and bending-torsion
D_{ij}	The stiffness of bending and torsion
E	The elastic constant
F_{ij}	The stiffness of transverse shears
f	The load function for anisotropic material
J'_1, J'_2, J'_3	The three basic invariants of the IPE deviatoric stress tensor
$d\varepsilon_{ij}^{p}$	The plastic strain tensor
L_{ijkl}	The invariant fourth-order transformation tensor
$M_{x,y}$	The bending-torsional moments
$N_{x,y}$	The membrane forces
[Q]	The in-plane elastic matrix
S_{ijkl}	The orthotropic elastic compliance tensor
$T_{x,y}$	The transverse shear forces on a plate
u, v	The displacements of the membrane in the plane z = 0

Table 1 Description of symbol (continued)

Sign	Symbol description
w	The transverse displacement
σ_y	The plasticity threshold
β_x	The rotation of the x, y plane around y
β_y	The rotation of the x, y plane around x
$\{e^*\}$	The vector of membrane deformations
$\{\kappa^*\}$	The vector of curvatures
$\{\gamma\}$	The transverse shear strain vector

2.2. *Theoretical formulations*

Cardboard is comprised of many layers of paper (Fig. 1). The manufacturing process furnishes with three characteristic directions: the machine direction (MD), the cross direction (CD), and the ZD, in which each layer of paper exhibits quite complex anisotropic and non-linear behavior. To study the general behavior of cardboard, the behavior of each layer of cardboard is putatively indispensable to be clarified. Mäkelä and Östlund [17] proposed a model to study the elastic-plastic behavior of paper. Accordingly, in the IPE model, the definition of the deviatoric stress tensor J'_2 is modified to suit the paper material [30].

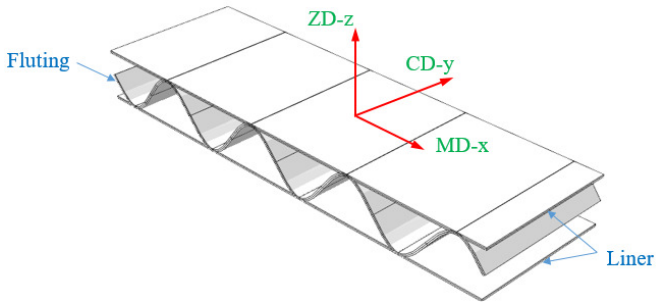

Fig. 1 Geometric structure and the directions of the corrugated cardboard

The components of the deviatoric stress tensor, s_{ij}, are defined by:

$$s_{ij} = L_{ijkl}\sigma_{kl} \tag{1}$$

where L denotes an invariant fourth-order transformation tensor, and it satisfies the symmetry conditions given by:

$$L_{ijkl} = L_{jikl} = K_{klij} \tag{2}$$

The following equations pertain to the properties of an orthotropic material.

$$s' = L\sigma = \begin{bmatrix} S'_{11} \\ S'_{22} \\ S'_{33} \\ S'_{12} \\ S'_{23} \\ S'_{31} \end{bmatrix} = \frac{1}{3}\begin{bmatrix} 2A & C-A-B & B-C-A & 0 & 0 & 0 \\ C-A-B & 2B & A-B-C & 0 & 0 & 0 \\ B-C-A & A-B-C & 2C & 0 & 0 & 0 \\ 0 & 0 & 0 & 3D & 0 & 0 \\ 0 & 0 & 0 & 0 & 3E & 0 \\ 0 & 0 & 0 & 0 & 0 & 3F \end{bmatrix}\begin{bmatrix} \sigma_{11} \\ \sigma_{22} \\ \sigma_{33} \\ \sigma_{12} \\ \sigma_{23} \\ \sigma_{31} \end{bmatrix} \tag{3}$$

The three basic invariants of the IPE deviatoric stress tensor are given by:

$$\begin{cases} J'_1 = s'_{kk} = 0 \\ J'_2 = \dfrac{1}{2} s'_{ij}\, s'_{ji} \\ J'_3 = \dfrac{1}{3} s'_{ij}\, s'_{jk}\, s'_{ki} \end{cases} \tag{4}$$

Using the second invariant of the IPE deviatoric stress tensor:

$$\sigma'_e = \sqrt{3J'_2} \tag{5}$$

Concerning the IPE material and the anisotropic material, the plastic strain tensor increases gradually and is represented by:

$$d\varepsilon_{ij}^p = L_{ijkl} d\varepsilon'^p_{kl} \tag{6}$$

and the corresponding work-equivalent incremental plastic strain tensor is given by:

$$d\varepsilon'^p_e = \sqrt{\frac{2}{3} d\varepsilon'^p_{ij}\, d\varepsilon'^p_{ij}} \tag{7}$$

The load function for anisotropic material then becomes:

$$f' = \sigma'_e - H' = \sigma'_e - E_0 \left(\varepsilon'^p_e\right)^{\frac{1}{n}} \tag{8}$$

The expression for the plastic strain increment can be expressed as

$$d\varepsilon_{ij}^p = \frac{\partial \sigma'_e}{\partial \sigma_{ij}} \frac{\partial \sigma'_e}{\partial \sigma_{kl}} d\sigma_{kl} \Bigg/ \frac{\partial H'}{\partial \varepsilon'^p_e} \frac{\partial \varepsilon'^p_e}{\partial \varepsilon^p_{mn}} \frac{\partial \sigma'}{\partial \sigma_{mn}} \tag{9}$$

The orthotropic elastic-plastic deformation stiffness is given by

$$d\varepsilon_{ij} = S_{ijkl} d\sigma_{kl} + \frac{9n\left(\sigma'_e\right)^{n-3}}{4E_0^n} L_{ijop} s'_{op} L_{ijop} s'_{qr} d\sigma_{kl},\ if\ f = 0\ and\ d\sigma'_e > 0 \tag{10}$$

$$d\varepsilon_{ij} = S_{ijkl} d\sigma_{kl},\ if\ f < 0\ or\ if = 0\ and\ d\sigma'_e \le 0 \tag{11}$$

where S_{ijkl} is the orthotropic elastic compliance tensor. Finally, the law of behavior in orthotropic linear elasticity in-plane constraints is written:

$$\{\sigma\} = \begin{Bmatrix} \sigma_x \\ \sigma_y \\ \sigma_{xy} \end{Bmatrix} = [H]\{\varepsilon^e\} = \frac{1}{\left(1 - v_{xy} v_{yx}\right)} \begin{pmatrix} E_x & v_{yx} E_x & 0 \\ v_{xy} E_y & E_y & 0 \\ 0 & 0 & G_{xy}\left(1 - v_{xy} v_{yx}\right) \end{pmatrix} \begin{Bmatrix} \varepsilon_x^{\,e} \\ \varepsilon_y^{\,e} \\ \gamma_{xy}^{\,e} \end{Bmatrix} \tag{12}$$

In the IPE model, a fictitious isotropic material has a stress state equal to the corresponding stress state in a real anisotropic material. The isotropic relationship between the deviatoric stress tensor and the stress tensor is expressed as follows:

$$\{s\} = \begin{Bmatrix} s_x \\ s_y \\ s_z \\ s_{xy} \end{Bmatrix} = [L]\{\sigma\} = \frac{1}{3} \begin{pmatrix} 2A & C - A - B & 0 \\ C - A - B & 2B & 0 \\ B - C - A & A - B - C & 0 \\ 0 & 0 & 3D \end{pmatrix} \begin{Bmatrix} \sigma_x \\ \sigma_y \\ \sigma_{xy} \end{Bmatrix} \tag{13}$$

Load function, the flow or normality law, the equivalent plastic strain increment, and the consistency equation are given respectively by the following expressions:

$$f = \sigma_{eq} - \sigma_y = \left(\frac{3}{2} < s > \{s\}\right)^{\frac{1}{2}} - E_0 \left(\varepsilon_0 + \varepsilon_{eq}^p\right)^{\frac{1}{n}} \tag{14}$$

$$\{d\varepsilon^p\} = d\lambda \left(\frac{\partial f}{\partial \{\sigma\}}\right) = \Lambda\{a\} \tag{15}$$

$$d\varepsilon_{eq}^{p} = \sqrt{\frac{2}{3} < d\varepsilon^{p} > \{d\varepsilon^{p}\}} = d\lambda = \Lambda \tag{16}$$

$$f = \left(\frac{\partial f}{\partial \{\sigma\}}\right)^{T} d\{\sigma\} - \frac{\partial f}{\partial \varepsilon_{eq}^{p}} d\varepsilon_{eq}^{p} = < a > d\{\sigma\} - \sigma_{y}' \Lambda \tag{17}$$

where σ_y is the plasticity threshold, A, B, C, D, E_0, and n are the parameters of the IPE model, which can be identified from the experimental traction curves. The model will be implemented in the Abaqus/Explicit software using the VUMAT user subroutine (Fig. 2).

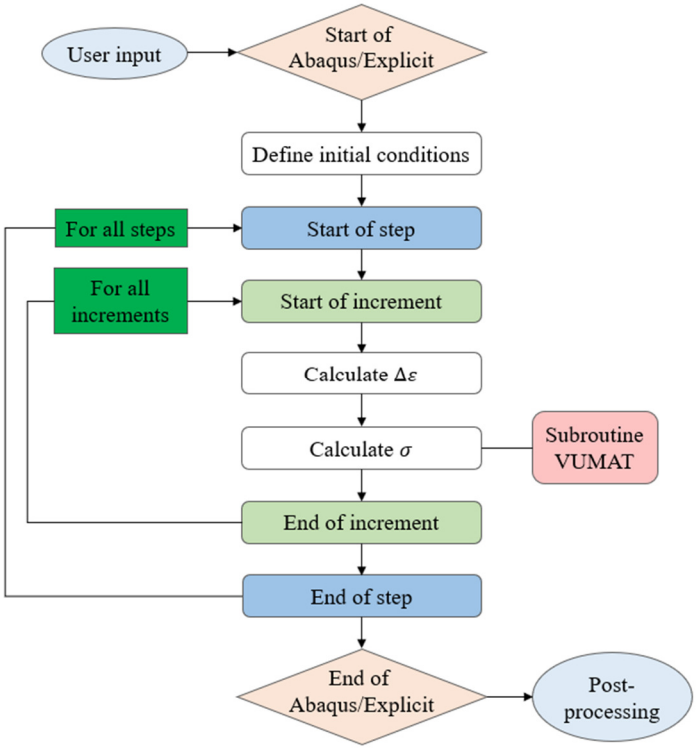

Fig. 2 Analysis in Abaqus/Explicit uses the VUMAT user subroutine

Cardboard panels render a multi-layer structure, hence, when studying their behavior, using the theory for thick panels or composite panels such as Hencky-Mindlin's theory and the multi-layer plate theory is incumbent herein. The Hencky-Mindlin theory considers the effect of cross-sectioning. According to Hencky theory:

$$\begin{cases} u = z\beta_x(x, y) \\ v = z\beta_y(x, y) \\ w = w(x, y) \end{cases} \tag{18}$$

$$\begin{cases} \varepsilon_x = z\dfrac{\partial \beta_x}{\partial_x} \\ \varepsilon_y = z\dfrac{\partial \beta_y}{\partial_y} \\ 2\varepsilon_{xy} = \gamma_{xy} = z\left(\dfrac{\partial \beta_x}{\partial_y} + \dfrac{\partial \beta_y}{\partial_x}\right) \\ 2\varepsilon_{xz} = \gamma_{xz} = \beta_x + \dfrac{\partial_w}{\partial_x} \\ 2\varepsilon_{yz} = \gamma_{yz} = \beta_y + \dfrac{\partial_w}{\partial_y} \end{cases} \tag{19}$$

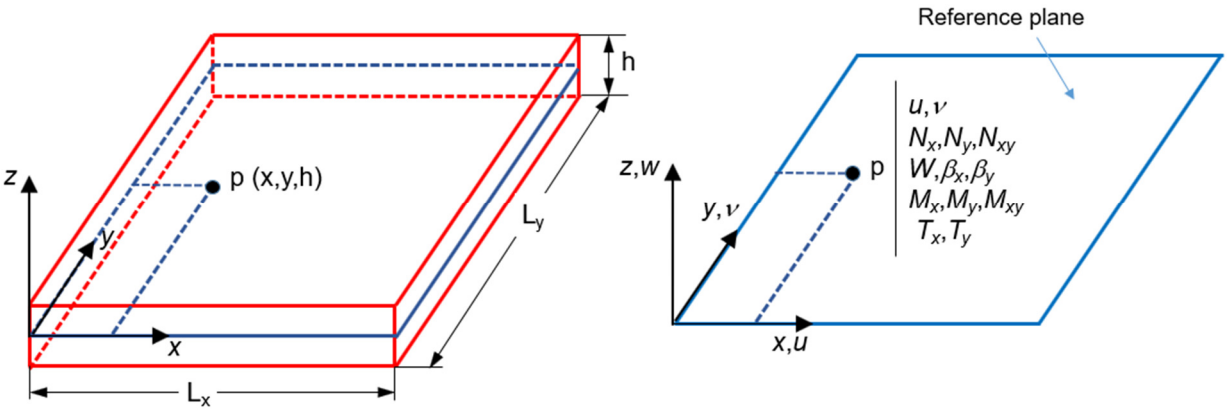

Fig. 3 Mechanical characteristics of a flat plate

Consider the geometric and mechanical characteristics of a flat plate, as shown in Fig. 3. Where u and v are the displacements of the membrane in the plane z = 0, w the transverse displacement, β_x the rotation of the x, y plane around y, β_y the rotation of the x, y plane around x. The membrane forces, the bending, and torsion moments are established as follows:

$$N_x = \int_{-h/2}^{h/2} \sigma_x dz,\ N_y = \int_{-h/2}^{h/2} \sigma_y dz,\ N_{xy} = \int_{-h/2}^{h/2} \sigma_{xy} dz \tag{20}$$

$$M_x = \int_{-h/2}^{h/2} \sigma_x z dz,\ M_y = \int_{-h/2}^{h/2} \sigma_y z dz \tag{21}$$

$$T_x = \int_{-h/2}^{h/2} \sigma_{xz} z dz,\ T_y = \int_{-h/2}^{h/2} \sigma_{yz} z dz \tag{22}$$

According to Mindlin's theory, the following virtual displacement field of a point q is presented as:

$$u_q^* = u^* + z\beta^* \tag{23}$$

$$\begin{Bmatrix} u^*(x,y,z) \\ v^*(x,y,z) \\ w^*(x,y,z) \end{Bmatrix} = \begin{Bmatrix} u^*(x,y) \\ v^*(x,y) \\ w^*(x,y) \end{Bmatrix} + z \begin{Bmatrix} \beta^*(x,y) \\ \beta^*(x,y) \\ 0 \end{Bmatrix} \tag{24}$$

$$\{\varepsilon^*\} = \{e^*\} + z\{\kappa^*\} \tag{25}$$

where $\{e^*\}$ is the vector of membrane deformations and $\{\kappa^*\}$ is the vector of curvatures.

$$\begin{cases} \{\varepsilon^*\} = \begin{bmatrix} \varepsilon_x^* \\ \varepsilon_y^* \\ 2\varepsilon_{xy}^* \end{bmatrix} = z\{\kappa^*\} \\ \{e^*\} = \begin{bmatrix} u_x^* \\ v_y^* \\ v_x^* + v_y^* \end{bmatrix} \\ \{\kappa^*\} = \begin{bmatrix} \beta_{x,x}^* \\ \beta_{y,y}^* \\ \beta_{x,y}^* + \beta_{y,x}^* \end{bmatrix} \\ \{\gamma^*\} = \begin{bmatrix} \beta_x^* + w_x^* \\ \beta_y^* + w_y^* \end{bmatrix} \end{cases} \tag{26}$$

The elastic constitutive law for an orthotropic material is written as:

$$\{\sigma\}=\begin{Bmatrix}\sigma_x\\ \sigma_y\\ \sigma_{xy}\end{Bmatrix}=[Q]\begin{Bmatrix}\varepsilon_x^*\\ \varepsilon_y^*\\ \varepsilon_{xy}^*\end{Bmatrix}=\begin{bmatrix}E_x/1-v_{xy}v_{yx} & v_{xy}E_y/1-v_{xy}v_{yx} & 0\\ v_{yx}E_x/1-v_{xy}v_{yx} & E_y/1-v_{xy}v_{yx} & 0\\ 0 & 0 & G_{xy}\end{bmatrix}\begin{Bmatrix}\varepsilon_x^*\\ \varepsilon_y^*\\ \gamma_{xy}^*\end{Bmatrix} \tag{27}$$

$$\{\sigma_\gamma\}=\begin{Bmatrix}\sigma_{xz}\\ \sigma_{yz}\end{Bmatrix}=[C]\begin{Bmatrix}\gamma_{zx}^*\\ \gamma_{yz}^*\end{Bmatrix}=\begin{bmatrix}G_{xz} & 0\\ 0 & \sigma_{yz}\end{bmatrix}\begin{Bmatrix}\gamma_{zx}^*\\ \gamma_{yz}^*\end{Bmatrix} \tag{28}$$

According to the multi-layer plate theory, a composite panel consisting of many layers (Fig. 4), and the multi-layer panel theory, the previously determined forming forces are accumulated layer by layer to achieve the relationships.

$$\begin{Bmatrix}N_x\\ N_y\\ N_{xy}\end{Bmatrix}=\int_{-h/2}^{h/2}\begin{Bmatrix}\sigma_x\\ \sigma_y\\ \sigma_{xy}\end{Bmatrix}dz=\sum_{k=1}^{n}\int_{k-1}^{k}\begin{pmatrix}Q_{11} & Q_{12} & 0\\ Q_{12} & Q_{22} & 0\\ 0 & 0 & Q_{23}\end{pmatrix}_k\left(\begin{Bmatrix}\varepsilon_x\\ \varepsilon_y\\ \gamma_{xy}\end{Bmatrix}+z\begin{Bmatrix}\kappa_x\\ \kappa_y\\ \kappa_{xy}\end{Bmatrix}\right)dz \tag{29}$$

$$\begin{Bmatrix}M_x\\ M_y\\ M_{xy}\end{Bmatrix}=\int_{-h/2}^{h/2}\begin{Bmatrix}\sigma_x\\ \sigma_y\\ \sigma_{xy}\end{Bmatrix}zdz=\sum_{k=1}^{n}\int_{k-1}^{k}\begin{pmatrix}Q_{11} & Q_{12} & 0\\ Q_{12} & Q_{22} & 0\\ 0 & 0 & Q_{23}\end{pmatrix}_k\left(z\begin{Bmatrix}\varepsilon_x\\ \varepsilon_y\\ \gamma_{xy}\end{Bmatrix}+z^2\begin{Bmatrix}\kappa_x\\ \kappa_y\\ \kappa_{xy}\end{Bmatrix}\right)dz \tag{30}$$

$$\begin{Bmatrix}T_x\\ T_y\end{Bmatrix}=\int_{-h/2}^{h/2}\begin{Bmatrix}\sigma_{xz}\\ \sigma_{yz}\end{Bmatrix}dz=\sum_{k=1}^{n}\int_{k-1}^{k}\begin{pmatrix}C_{11} & 0\\ 0 & C_{22}\end{pmatrix}_k\begin{Bmatrix}\gamma_{xz}\\ \gamma_{yz}\end{Bmatrix}dz \tag{31}$$

After the integration, according to the thickness, one obtains the matrix of the total rigidities which binds the generalized deformations to the resulting efforts:

$$\begin{Bmatrix}N_x\\ N_y\\ N_{xy}\\ M_x\\ M_y\\ M_{xy}\\ T_x\\ T_y\end{Bmatrix}=\begin{bmatrix}A_{11} & A_{12} & 0 & B_{11} & B_{12} & 0 & 0 & 0\\ A_{12} & A_{22} & 0 & B_{12} & B_{22} & 0 & 0 & 0\\ 0 & 0 & A_{23} & 0 & 0 & B_{33} & 0 & 0\\ B_{11} & B_{12} & 0 & D_{11} & D_{12} & 0 & 0 & 0\\ B_{12} & B_{22} & 0 & D_{12} & D_{22} & 0 & 0 & 0\\ 0 & 0 & B_{11} & 0 & 0 & D_{33} & 0 & 0\\ 0 & 0 & 0 & 0 & 0 & 0 & F_{11} & 0\\ 0 & 0 & 0 & 0 & 0 & 0 & 0 & F_{22}\end{bmatrix}\begin{Bmatrix}\varepsilon_x\\ \varepsilon_y\\ \gamma_{xy}\\ \kappa_x\\ \kappa_y\\ \kappa_{xy}\\ \gamma_{xz}\\ \gamma\end{Bmatrix} \tag{32}$$

The terms A_{ij}, B_{ij}, and D_{ij} represent the stiffness of the membrane, the coupling between membrane and bending-torsion, and the stiffness of bending and torsion, respectively. Similarly, F_{ij} represents the stiffness of transverse shears. These terms are defined in the formula below.

$$A_{ij}=\sum_{k=1}^{n}\left[h^k-h^{k-1}\right]Q_{ij}^k=\sum_{k=1}^{n}Q_{ij}^k t^k \tag{33}$$

$$B_{ij}=\frac{1}{2}\sum_{k=1}^{n}\left[(h^k)^2-(h^{k-1})^2\right]Q_{ij}^k=\sum_{k=1}^{n}Q_{ij}^k t^k z^k \tag{34}$$

$$D_{ij}=\frac{1}{3}\sum_{k=1}^{n}\left[(h^k)^3-(h^{k-1})^3\right]Q_{ij}^k=\sum_{k=1}^{n}Q_{ij}^k\left[t^k(z^k)^2+\frac{(t^k)^3}{12}\right] \tag{35}$$

$$F_{ij}=\sum_{k=1}^{n}\left[h^k-h^{k-1}\right]C_{ij}^k=\sum_{k=1}^{n}C_{ij}^k t^k \tag{36}$$

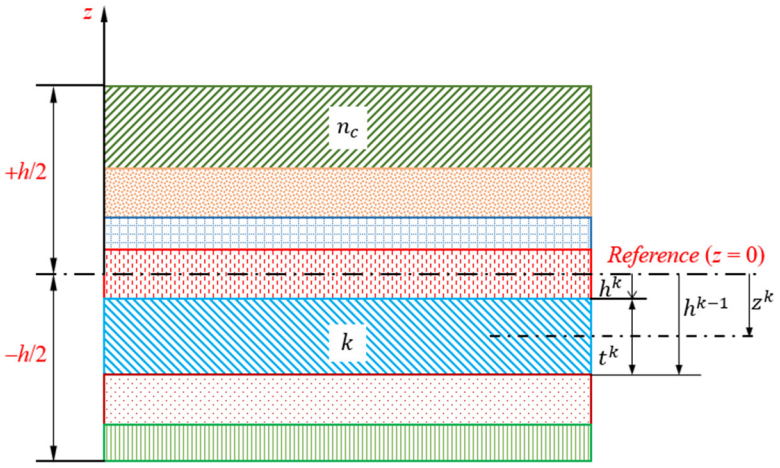

Fig. 4 Multi-layer panels

3. Solution Procedures

Homogenization is the cardinal research method used in this paper and is used to build an equivalent 2D elastic-plastic finite element model. Using the UGENS subroutine, this 2D model is implemented into the Abaqus software. Research shows that determining the values of parameters in the material behavior model is crucial. Hence, an inverse identification procedure is proposed to determine these values.

3.1. Homogenization method

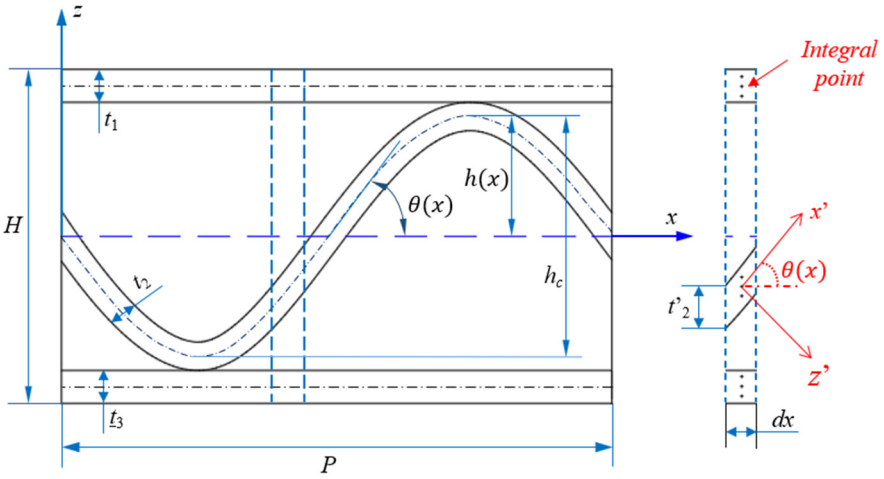

Fig. 5 Periodic unit cell of a corrugated cardboard

To analyze the behavior of corrugated core cardboard panels, a homogenization technique is proposed based on shell panel theory, multi-layer panel theory, and theories for composite panels. The homogenization method is carried out with a representative element, as shown in Fig. 5. The size of this periodic unit cell should be ideally adequate to represent the plate and be comparable to the entire plate. The mechanical properties of the periodic unit cell will be used to model the 3D structure using an equivalent 2D plate. Accordingly, the relationship between the size components is as follows:

$$h(x) = \frac{h_c}{2}\sin\left(\frac{2\pi x}{P}\right);\ \theta(x) = \arctan\left(\frac{dh(x)}{dx}\right) \tag{37}$$

Regarding each layer of paper (skin and flute), three points are determined to integrate through the thickness. The plastic algorithm is applied at each integration point to determine the stress state and the elastic-plastic matrix in the local coordinate system of each layer. The corrugated core layer poses a decrease in elastic modulus in the x and y directions due to the influence of angle $\theta(x)$ [12]. The elastic constants for the fluting are calculated as follows:

$$E(\theta)_x = \frac{1}{\frac{\cos(\theta)^4}{E_1} + \left(\frac{1}{G_{12}} - \frac{2v_{12}}{E_1}\right)\cos(\theta)^2 \sin(\theta)^2 + \frac{\sin(\theta)^4}{E_2}} \tag{38}$$

$$E(\theta)_y = \frac{1}{\frac{\sin(\theta)^4}{E_1} + \left(\frac{1}{G_{12}} - \frac{2v_{12}}{E_1}\right)\cos(\theta)^2 \sin(\theta)^2 + \frac{\sin(\theta)^4}{E_2}} \tag{39}$$

$$v(\theta)_{xy} = E(\theta)_x \left[\frac{v_{12}}{E_1}\left(\cos(\theta)^4 + \sin(\theta)^4\right) - \left(\frac{1}{E_1} + \frac{1}{E_2} + \frac{1}{G_{12}}\right)\cos(\theta)^2 \sin(\theta)^2\right] \tag{40}$$

$$G(\theta)_{xy} = \frac{1}{2\left(\frac{2}{E_1} + \frac{2}{E_2} + \frac{4v_{12}}{E_1} - \frac{1}{G_{12}}\right)\cos(\theta)^2 \sin(\theta)^2 + \frac{\cos(\theta)^4 + \sin(\theta)^4}{G_{12}}} \tag{41}$$

Eqs. (33) to (36) are modified to be suitable for cardboard sheets:

$$[A] = \int_{-h/2}^{h/2} Q_{ij} dz \Rightarrow A_{ij} = \sum_{k=1}^{3} Q_{ij} t_k = Q_{ij}^{(1)} t_1 + Q_{ij}^{(2)}\left(\theta(x)\right) t_2 + Q_{ij}^{(3)} t_3 \tag{42}$$

$$[B] = \int_{-h/2}^{h/2} z Q_{ij} dz \Rightarrow B_{ij} = \sum_{k=1}^{3} Q_{ij} z_k t_k = Q_{ij}^{(1)} z_1 t_1 + Q_{ij}^{(2)}\left(\theta(x)\right) z_2 t_2 + Q_{ij}^{(3)} z_3 t_3 \tag{43}$$

$$\begin{aligned}[D] &= \int_{-h/2}^{h/2} z^2 Q_{ij} dz \Rightarrow D_{ij} = \sum_{k=1}^{3} Q_{ij}\left(z_k^2 t_k + \frac{1}{12} t_k^3\right) \\ &= Q_{ij}^{(1)}\left(z_1^2 t_1 + \frac{1}{12} t_1^3\right) + Q_{ij}^{(2)}\left(z_2^2 t_2^{'} + \frac{1}{12}(t_2^{'})^3\right) + Q_{ij}^{(3)}\left(z_3^2 t_3 + \frac{1}{12} t_3^3\right)\end{aligned} \tag{44}$$

$$F_{ij} = \frac{5}{6}\left[C_{ij}^{(1)} t_1 + C_{ij}^{(2)}\left(\theta(x)\right) t_2 + C_{ij}^{(3)} t_3\right] \tag{45}$$

where

$$t_2 = \frac{t_2}{\cos\theta(x)} \tag{46}$$

The average stiffness of all slices in the sinusoidal period P, in the MD direction, is calculated according to the formulas:

$$A_{ij}^H = \frac{1}{P}\int_0^P A_{ij}(x) dx \tag{47}$$

$$B_{ij}^H = \frac{1}{P}\int_0^P B_{ij}(x) dx \tag{48}$$

$$D_{ij}^H = \frac{1}{P}\int_0^P D_{ij}(x) dx \tag{49}$$

$$F_{ij}^H = \frac{1}{P}\int_0^P F_{ij}(x) dx \tag{50}$$

The simplifying hypotheses as well as the calculations of the different rigidities are given in Duong [19]. The plasticity algorithm developed (IPE model) for each integration point at each layer is used. Accordingly, the stress state and tangent matrix are updated after each increase. The membrane force, bending, and torsional moments are obtained by integrating the stresses over the thickness of the plate by replacing the elastic matrix $[Q_{(k)}]$ with the tangential matrix $[Q_{p(k)}]$ in Eqs. (42)-(44) to obtain the overall stiffness matrix:

$$A_{ij}(x)=\frac{t_1}{2}\sum_{k=1}^{3}Q_{pij}^{(1)}w_k+\frac{t_2}{2}\sum_{k=1}^{3}Q_{pij}^{(2)}\left(\theta(x)\right)w_k+\frac{t_3}{2}\sum_{k=1}^{3}Q_{pij}^{(3)}w_k \tag{51}$$

$$B_{ij}(x)=\frac{t_1}{2}\sum_{k=1}^{3}Q_{pij}^{(1)}z_k w_k+\frac{t_2}{2}\sum_{k=1}^{3}Q_{pij}^{(2)}\left(\theta(x)\right)z_k w_k+\frac{t_3}{2}\sum_{k=1}^{3}Q_{pij}^{(3)}z_k w_k \tag{52}$$

$$D_{ij}(x)=\frac{t_1}{2}\sum_{k=1}^{3}Q_{pij}^{(1)}z_k^2 w_k+\frac{t_2}{2}\sum_{k=1}^{3}Q_{pij}^{(2)}\left(\theta(x)\right)z_k^2 w_k+\frac{t_3}{2}\sum_{k=1}^{3}Q_{pij}^{(3)}z_k^2 w_k \tag{53}$$

Notably, the carton is symmetrical concerning its mean surface so B_{ij} = 0, and the integral variable *dx* will affect the convergence of the solution [16]. Therefore, *dx* will choose the value 0.005 mm

3.2. Method for determining material parameters in the elastic-plastic model

The inverse determination method was used to determine the parameters in the IPE model. The method is carried out by running finite element simulations of tensile tests at MD, CD, and 45° and then comparing the results obtained with the experimental results. The quadratic difference between the numerical result and the experimental result is given by the objective function:

$$F_{obj}=\frac{1}{N}\sum_{i=1}^{N}\left[F_{\text{num}}\left(U_{\text{num}}\right)-F_{\text{exp}}\left(U_{\text{exp}}\right)\right]^2 \tag{54}$$

where N is the number of the data set, U_{num} and U_{exp} are the numerical displacement and experimental displacement, and F_{num} and F_{exp} are the indenter forces numerically computed and experimentally measured, respectively.

Currently, a legion of standard optimization algorithms, such as Simplex, Multi-Objective Genetic Algorithm II (MOGA-II), and Levenberg-Marquardt as well as advanced optimization algorithms like Multi-Objective Simulated Annealing (MOSA) and Non-dominated Sorting Genetic Algorithm II (NSGA-II) are available and can be used depending on the complexity of the problem to be solved. In this study, the genetic optimization algorithm MOGA-II to minimize the objective function in Eq. (54), is used. The MOGA-II genetic algorithm will update the parameter set of the IPE model during the optimization process. The inverse determination procedure is summarized in Fig. 6. The accuracy of the results will be presented in the following section.

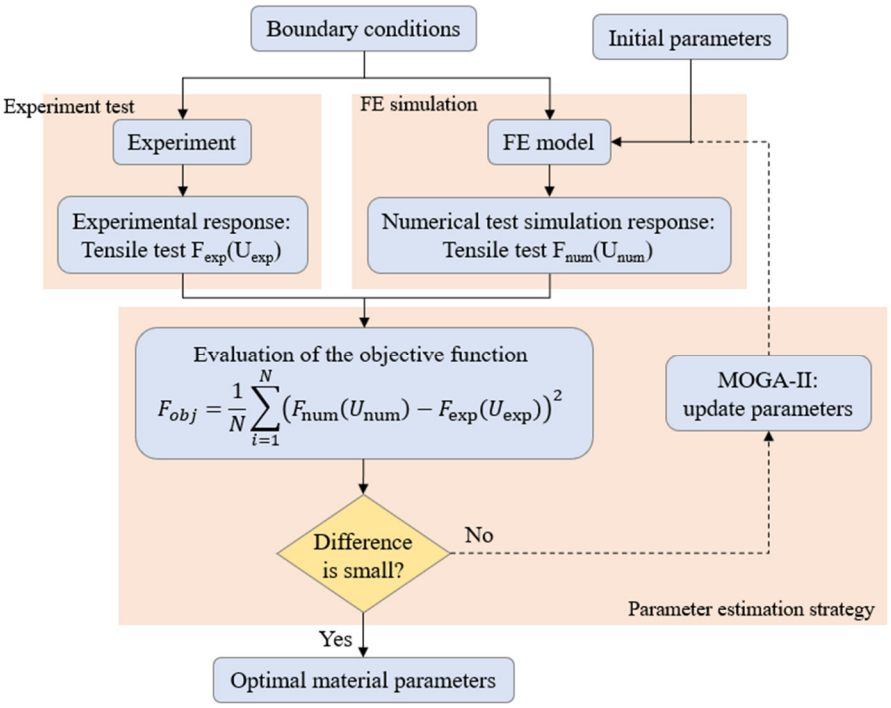

Fig. 6 Identification method by the inverse method

4. Results and Discussions

In this section, the inverse identification process proposed in the erstwhile section is applied to determine the parameter values of the IPE behavior model of paper material. The numerical simulations for the proposed 3D model and 2D model were conducted herein. The accuracy of the proposed model is evaluated by comparing the results obtained between the two models.

4.1. Determine material parameters in the equivalent elastic-plastic model

Cardboard is one of the typical sandwich structures. The material used in this study is type B cardboard with geometric structure and properties, as shown in Fig. 7 and Table 2. The inverse identification process is applied in the previous section to determine the parameter values in the IPE behavior model of the material paper in this study. The obtained elastic and plastic properties are shown in Table 3 and Table 4 respectively.

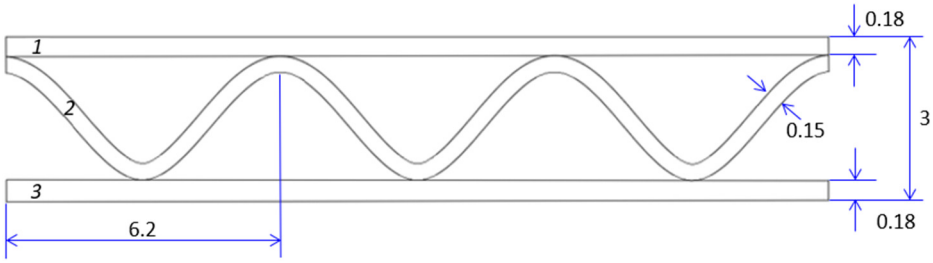

Fig. 7 Geometric structure of the corrugated cardboard plate (mm)

Table 2 Cardboard plate properties

	Grammage (g/mm^2)	Thickness (mm)
Liner	140	0.18±0.004
Fluting	113	0.15±0.008
Liner	140	0.18±0.004

Table 3 Elastic properties of the cardboard plates

	E_x (MPa)	E_y (MPa)	v_{xy}	G_{xy} (MPa)	E_0
Liners	2350.2	879.91	0.0829	1047.2	91.45
Fluting	1120.4	615.85	0.0717	301.05	80.31

Table 4 Plastic properties of the cardboard plates

	n	A	B	C	D
Liners	3.807	1.0	2.136	2.136	1.422
Fluting	3.047	1.0	2.718	2.136	1.571

4.2. Validation of the equivalence model

Evaluation of the accuracy of the proposed equivalent 2D model is performed by analyzing the stress-strain changes and acceleration responses in the 3D and 2D models of corrugated core cardboard panels. Static and dynamic load cases such as tensile, cyclic, and impact loads. Furthermore, the advantages of the equivalent 2D model are demonstrated through reduced calculation time compared to the 3D model.

4.2.1. Numerical simulation of tensile test on specimen notched

Numerical simulations of the tensile specimen in the MD, CD, and 45° directions, for the 3D model and the equivalent 2D model, are performed. The dimensions of the specimen are shown in Fig. 8. Accordingly, one end of the sample is clamped tightly, and a tensile force is applied to the other end. The UGENS subroutine and the 4-node shell element S4R (with a mesh size of 0.5 mm) with three displacements, and three rotations were used in numerical simulation using Abaqus software. The results obtained are shown in Fig. 9. The behavior of both specimens is expressed through the relationship between force

versus elongation. During the elastic deformation stage, the results, which are obtained from the two models, are almost identical, while the experimental and simulation results are almost identical. During the plastic stage, the progression of accumulated plastic deformation in the two models is subtly different. This difference is due to the influence of the wavy core in the structure. This influence will be further analyzed in the following section. The results obtained initially confirm the reliability of the proposed model.

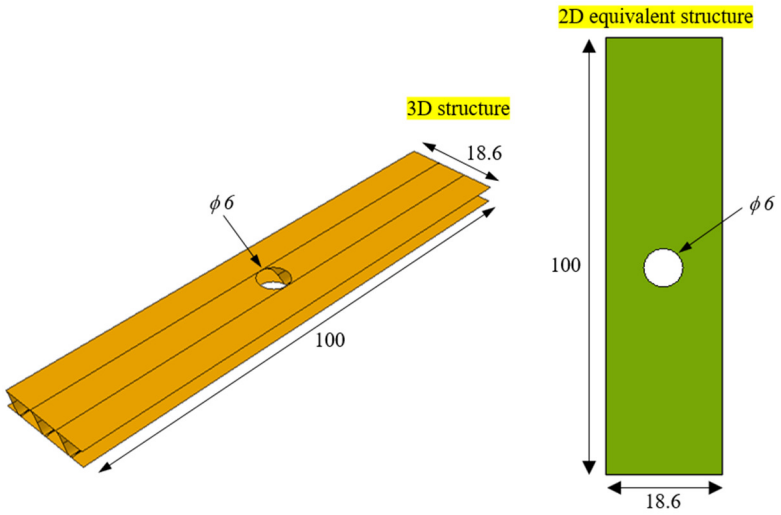

Fig. 8 Corrugated cardboard 3D structure and equivalent 2D model (mm)

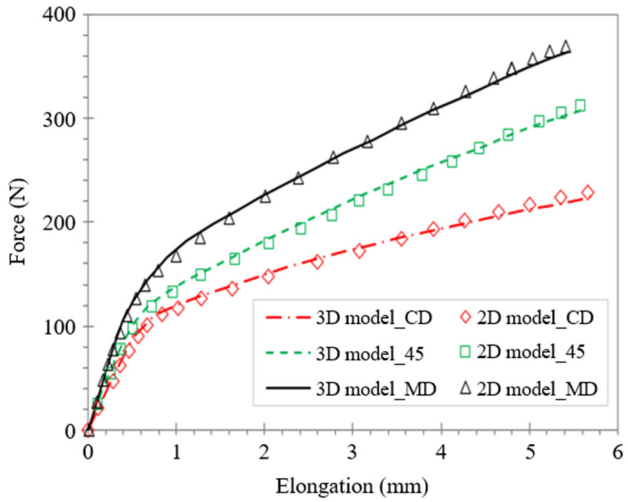

Fig. 9 Force and longitudinal strain in MD, CD, and 45° direction

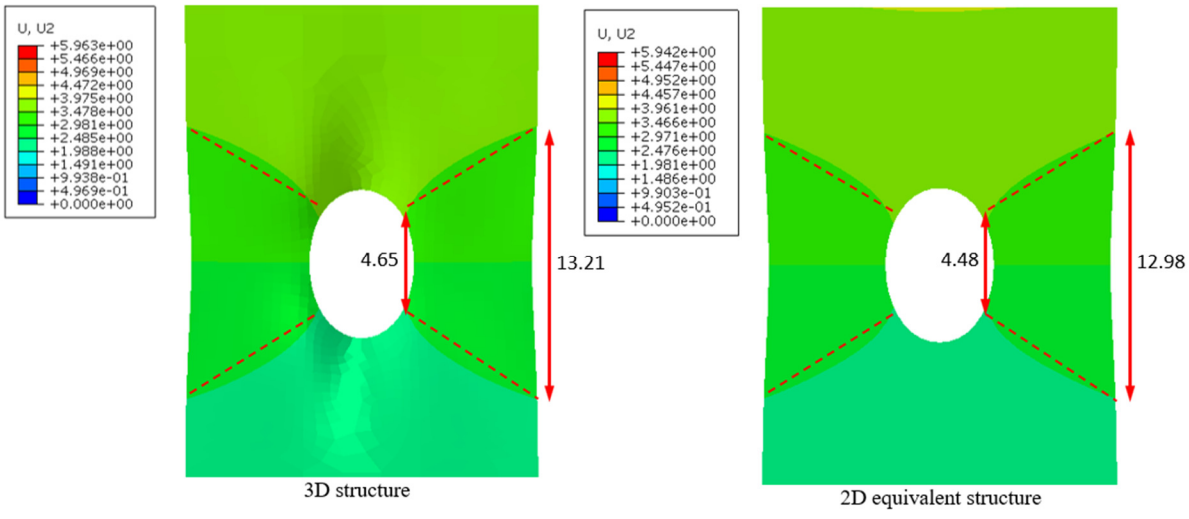

Fig. 10 Deformation at the hole location on the tensile specimen (mm)

Apropos the corrugated cardboard sheets, when applying tensile force in the MD direction, the corrugated core layer is all but not affected by the force. Therefore, in this section, the stress and deformation of cardboard plates subjected to tension in the CD direction are analyzed. To observe the variation of strain in the equivalent model, the strain around the hole on the tensile sample in the CD direction is analyzed. Fig. 10 indicates that the strain distribution at the hole location in the two models is identical. The hole edge deformation length is 4.65 mm and 4.48 mm for 3D and 2D models, respectively. Likewise, regarding the outer edge, the deformation is 13.21 mm and 12.98 mm for 3D and 2D models, respectively.

A comparison of the CPU time of the two models is depicted in Table 5. Numerical simulations are performed with a computer with the following configuration: Processor Intel(R) Xeon(R) CPU E5-2689 @ 2.60GHz 2.60 GHz, RAM 16.0 GB. Accordingly, when using a 2D model, the calculation time is reduced by 3.51 times (in the MD direction), 2.72 times (in the 45° direction), and 5.93 times (in the CD direction).

Table 5 Comparison of the CPU time

Direction	Times CPU (s)		Errors
	Model 3D	Model 2D	
MD	650	185	3.51 times
45°	1,357	498	2.72 times
CD	920	155	5.93 times

To confirm the accuracy of the elastic-plastic homogeneous model, an analysis of the longitudinal stress variation at the right edge of the hole is conducted to evaluate the evolution of the stress concentration coefficient, K_t, as a function of distance from the edge of the hole. The overstress coefficient K_t is determined by the ratio between the largest overstress near the hole and the applied stress. Regarding the two models studied in this section, the difference in maximum overstress (maximum overstrain) in the plastic phase is observably negligible (Fig. 11). The comparison of a 3D model and 2D model responses indicates that the developed equivalent model can accurately reproduce the mechanical properties of the specimen with a hole while the CPU is significantly reduced.

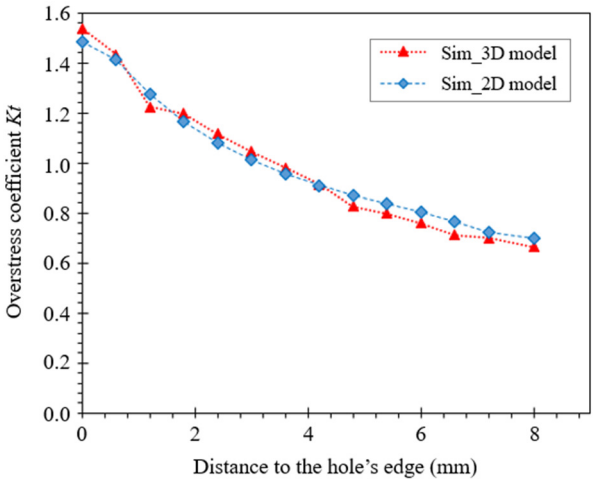

Fig. 11 Comparison of overstress profiles between the two models

4.2.2. Numerical simulation charge-discharge

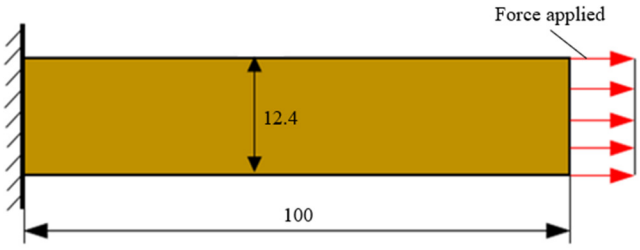

Fig. 12 Simulation of carton panels subjected to cyclic loading (mm)

The analysis of stress-strain variation in sandwich structures is performed by analyzing the simulation results of corrugated cardboard panels (3D model and 2D model), with dimensions as shown in Fig. 12, subjected to cyclic loading in the CD direction. Cyclic load with gradually increasing amplitude and steady amplitude is shown in Fig. 13.

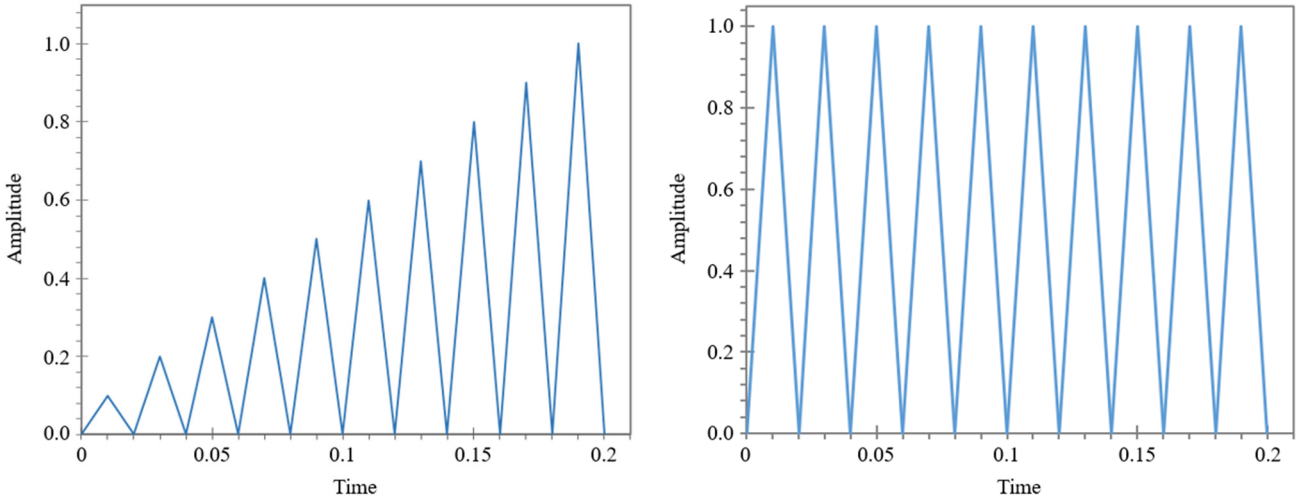

(a) Loading with increasing amplitude (b) Loading with stable amplitude

Fig. 13 Cyclic load

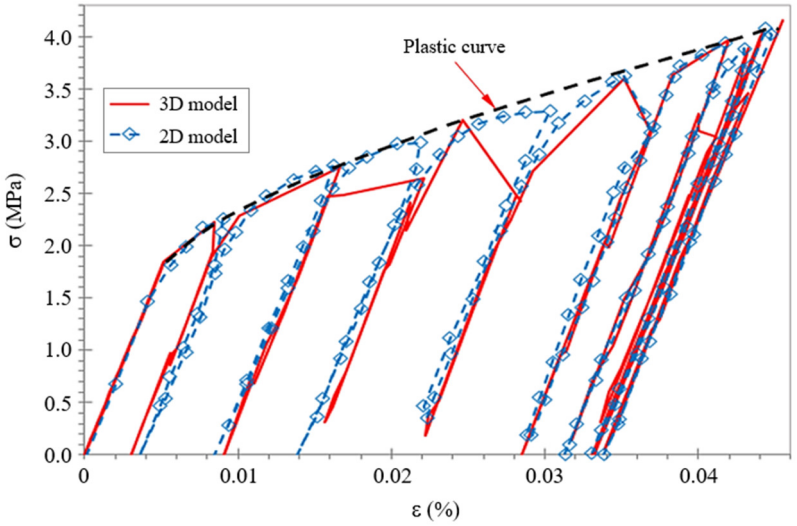

Fig. 14 Mechanical responses: 3D vs 2D model

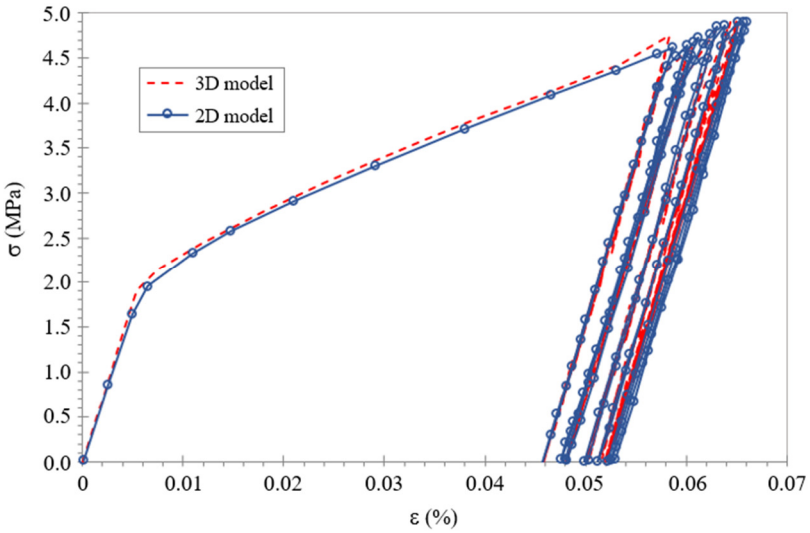

Fig. 15 Cyclic mechanical response: 3D vs 2D model

Concerning the case of loading with increasing amplitude, the results are obtained, as shown in Fig. 14. Apparently, the stress-strain variation in the two models is almost identical, whereas, in the first few cycles, the curve near the peak of each cycle renders several infinitesimal differences. Specifically, in the 3D model, the wavy core affects the displacement speed on the sample during each load-unloading time, causing the core to fold suddenly. The loading rate materially remains the same for each cycle, whereas after 20 cycles the strain rates in the two models decrease similarly, while the stress values are comparable. Apropos the case of applied load with stable amplitude, Fig. 15 shows that a nuanced difference emerges between the two models. In steady state, the stress and strain values vary each cycle by an acceptable extent. In particular, at the end of each cycle, the constraint value is equal to 0 for both models.

4.2.3. Numerical simulation of beams 3D and 2D subject to impact

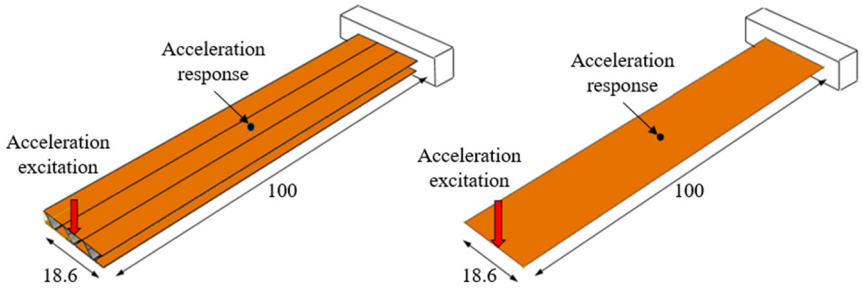

(a) Setup to simulate a plate subjected to impact loading (mm)

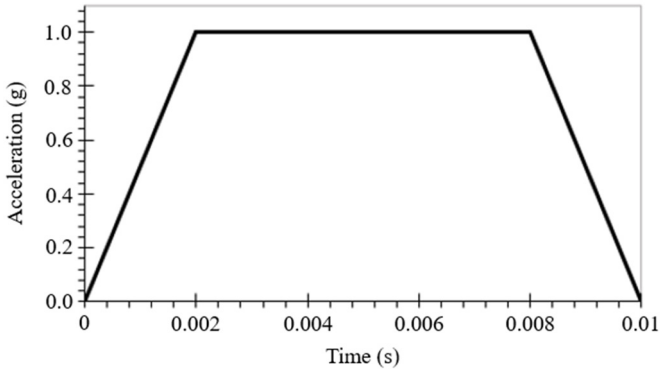

(b) Excitation pulse amplitude used for numerical simulation

Fig. 16 Numerical simulation of beams 3D and 2D subject to impact

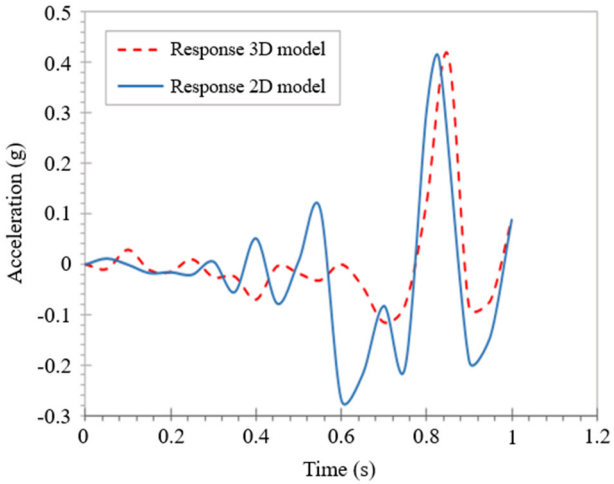

Fig. 17 Acceleration response comparison: 3D vs 2D model

Noticeably, the load-bearing beam is considered, as shown in Fig. 16(a). Acceleration at the free end of the beam for a short period (0.01s) is applied, and the response acceleration is measured at the midpoint of the beam. The FEM model, using S4R elements with a mesh size of 1mm, is created for both models. The 3D model consists of 7,397 elements and 7,067 nodes.

The 2D model includes 957 elements and 1,091 nodes. Excitation pulse amplitude is used for numerical simulation, as mentioned in Fig. 16(b). As shown in Fig. 17, the results obtained indicate the response acceleration obtained from the two models is similar. Meanwhile, acceleration response values and the CPU time are exhibited in Table 6. The difference in acceleration response acceleration value between the two models stands at less than 1.21% while the CPU time is reduced by 16.03 times.

Table 6 Comparison of the CPU time and acceleration response

	3D model	2D model	Error
Acceleration response (g)	0.41	0.405	1.21%
CPU time (s)	4,170	260	16.03 times

5. Conclusions

To investigate stress-strain in sandwich panel structures in general and corrugated core cardboard in particular, an equivalent 2D finite element model for corrugated core cardboard was built by using the homogenization method. The VUMAT and UGENS user subroutines were built to implement the paper IPE behavior model and the homogenization model in the Abaqus software. Model accuracy is confirmed by comparing the results of the 3D model and the equivalent 2D model. This study yields four remarks:

(1) The proposed model effectuates saving calculation time and reducing time for geometric model preparation, thereby saving costs in the process of designing corrugated core sandwich panels.
(2) The proposal has validated its effectiveness through its use as an alternative to 3D models to study stress-strain changes when structures are subjected to cyclic loading.
(3) The proposed model can be applied to other sandwich structures such as structures with trapezoidal and triangular cores.
(4) The proposed model is material for the calculation of carton boxes subjected to vibration and the impact during the transportation and distribution of goods.

Acknowledgments

This work was funded by the Ministry of Education & Training Vietnam (grant number B2023-TNA-20).

Conflicts of Interest

The authors declare no conflict of interest.

References

[1] Q. M. Shakir and H. K. Hannon, “Innovative Model of Precast RC Curved Hybrid Deep Beams Composed Partially With High-Performance Concrete,” Arabian Journal for Science and Engineering, vol. 49, no. 4, pp. 6045-6060, 2024.
[2] Q. M. Shakir and H. K. Hanoon, “New Models for Reinforced Concrete Precast Hybrid Deep Beams Under Static Loads With Curved Hybridization,” Structures, vol. 54, pp. 1007-1025, 2023.
[3] F. Xia, Y. Durandet, P. J. Tan, and D. Ruan, “Three-Point Bending Performance of Sandwich Panels With Various Types of Cores,” Thin-Walled Structures, vol. 179, article no. 109723, 2022.
[4] S. Vaidya, L. Zhang, D. Maddala, R. Hebert, J. T. Wright, A. Shukla, et al., “Quasi-Static Response of Sandwich Steel Beams With Corrugated Cores,” Engineering Structures, vol. 97, pp. 80-89, 2015
[5] M. R. M. Rejab and W. J. Cantwell, “The Mechanical Behaviour of Corrugated-Core Sandwich Panels,” Composites Part B: Engineering, vol. 47, pp. 267-277, 2013
[6] T. Garbowski and A. Knitter-Piątkowska, “Analytical Determination of the Bending Stiffness of a Five-Layer Corrugated Cardboard With Imperfections,” Materials, vol. 15, no. 2, article no. 663, 2022.
[7] M. Rogalka, J. K. Grabski, and T. Garbowski, “Deciphering Double-Walled Corrugated Board Geometry Using Image Analysis and Genetic Algorithms,” Sensors, vol. 24, no. 6, article no. 1772, 2024.

[8] J. Cillie and C. Coetzee, "Experimental and Numerical Investigation of the In-Plane Compression of Corrugated Paperboard Panels," Mathematical and Computational Applications, vol. 27, no. 6, article no. 108, 2022.
[9] K. Robertsson, E. Jacobsson, M. Wallin, E. Borgqvist, M. Ristinmaa, and J. Tryding, "A Continuum Damage Model for Creasing and Folding of Paperboard," Packaging Technology and Science, vol. 36, no. 12, pp. 1037-1050, 2023.
[10] F. M. Di Russo, M. M. Desole, A. Gisario, and M. Barletta, "Evaluation of Wave Configurations in Corrugated Boards by Experimental Analysis (EA) and Finite Element Modeling (FEM): The Role of the Micro-Wave in Packaging Design," The International Journal of Advanced Manufacturing Technology, vol. 126, no. 11-12, pp. 4963-4982, 2023.
[11] W. S. Chang, E. Ventsel, T. Krauthammer, and J. John, "Bending Behavior of Corrugated-Core Sandwich Plates," Composite Structures, vol. 70, no. 1, pp. 81-89, 2005.
[12] W. S. Chang, T. Krauthammer, and E. Ventsel, "Elasto-Plastic Analysis of Corrugated-Core Sandwich Plates," Mechanics of Advanced Materials and Structures, vol. 13, no. 2, pp. 151-160, 2006.
[13] N. Buannic, P. Cartraud, and T. Quesnel, "Homogenization of Corrugated Core Sandwich Panels," Composite Structures, vol. 59, no. 3, pp. 299-312, 2003.
[14] C. Pany, "An Insight on the Estimation of Wave Propagation Constants in an Orthogonal Grid of a Simple Line-Supported Periodic Plate Using a Finite Element Mathematical Model," Frontiers in Mechanical Engineering, vol. 8, article no. 926559, 2022.
[15] C. Pany, "Vibration Analysis of Curved Panels and Shell Using Approximate Methods and Determination of Optimum Periodic Angle," The International Conference on Advanced Mechanical and Power Engineering, pp. 354-365, 2021.
[16] N. Stenberg, "A Model for the Through-Thickness Elastic–Plastic Behaviour of Paper," International Journal of Solids and Structures, vol. 40, no. 26, pp. 7483-7498, 2003.
[17] P. Mäkelä and S. Östlund, "Orthotropic Elastic–Plastic Material Model for Paper Materials," International Journal of Solids and Structures, vol. 40, no. 21, pp. 5599-5620, 2003.
[18] Z. Aboura, N. Talbi, S. Allaoui, and M. L. Benzeggagh, "Elastic Behavior of Corrugated Cardboard: Experiments and Modeling," Composite Structures, vol. 63, no. 1, pp. 53-62, 2004.
[19] P. T. M. Duong, "Numerical Modeling of the Dynamic Behavior of Complex Packaging Structures by Homogenization Methods," Ph.D. dissertation, Université de Reims Champagne-Ardenne, 2012.
[20] V. D. Luong, A. S. Bonnin, F. Abbès, J. B. Nolot, D. Erre, and B. Abbès, "Finite Element and Experimental Investigation on the Effect of Repetitive Shock in Corrugated Cardboard Packaging," Journal of Applied and Computational Mechanics, vol. 7, no. 2, pp. 820-830, 2021.
[21] A. D. Hammou, P. T. M. Duong, B. Abbès, M. Makhlouf, and Y. Q. Guo, "Finite-Element Simulation with a Homogenization Model and Experimental Study of Free Drop Tests of Corrugated Cardboard Packaging," Mechanics & Industry, vol. 13, no. 3, pp. 175-184, 2012.
[22] D. Mrówczyński, A. Knitter-Piątkowska, and T. Garbowski, "Numerical Homogenization of Single-Walled Corrugated Board With Imperfections," Applied Sciences, vol. 12, no. 19, article no. 9632, 2022.
[23] Y. Xia, M. I. Friswell, and E. I. Saavedra Flores, "Equivalent Models of Corrugated Panels," International Journal of Solids and Structures, vol. 49, no. 13, pp. 1453-1462, 2012.
[24] Y. Zhang, Q. Chen, M. Wang, X. Zhang, and Z. Cai, "Plastic Forming of Sandwich Panels and Numerical Analyses of the Forming Processes Based on Elastoplastic Equivalent Model," Materials, vol. 14, no. 17, article no. 4955, 2021.
[25] K. E. Barrett, "The Finite Element Analysis of Homogeneous and Laminated Composite Plates Using a Simple Higher Order Theory," Communications in Applied Numerical Methods, vol. 4, no. 6, pp. 843-844, 1988.
[26] T. Garbowski, A. Knitter-Piątkowska, and D. Mrówczyński, "Numerical Homogenization of Multi-Layered Corrugated Cardboard With Creasing or Perforation," Materials, vol. 14, no. 14, article no. 3786, 2021.
[27] T. Garbowski and T. Gajewski, "Determination of Transverse Shear Stiffness of Sandwich Panels With a Corrugated Core by Numerical Homogenization," Materials, vol. 14, no. 8, article no. 1976, 2021.
[28] J. Park, S. Chang, and H. M. Jung, "Numerical Prediction of Equivalent Mechanical Properties of Corrugated Paperboard by 3D Finite Element Analysis," Applied Sciences, vol. 10, no. 22, article no. 7973, 2020.
[29] H. Li, L. Ge, B. Liu, H. Su, T. Feng, and D. Fang, "An Equivalent Model for Sandwich Panel With Double-Directional Trapezoidal Corrugated Core," Journal of Sandwich Structures & Materials, vol. 22, no. 7, pp. 2445-2465, 2020.
[30] A. P. Karafillis and M. C. Boyce, "A General Anisotropic Yield Criterion Using Bounds and a Transformation Weighting Tensor," Journal of the Mechanics and Physics of Solids, vol. 41, no. 12, pp. 1859-1886, 1993.